Analysis of high-energy x-ray diffraction data at high pressure: the case of vitreous As_2O_3 at 32 GPa

2007 J. Phys.: Condens. Matter 19 415103

(http://iopscience.iop.org/0953-8984/19/41/415103)

IOP PUBLISHING JOURNAL OF PHYSICS: CONDENSED MATTER

J. Phys.: Condens. Matter **19** (2007) 415103 (12pp) doi:10.1088/0953-8984/19/41/415103

Analysis of high-energy x-ray diffraction data at high pressure: the case of vitreous As_2O_3 at 32 GPa

Q Mei[1], C J Benmore[1], E Soignard[2], S Amin[2] and J L Yarger[2]

[1] Intense Pulsed Neutron Source and X-ray Science Divisions, Argonne National Laboratory, Argonne, IL 60439, USA
[2] Arizona State University, Department of Chemistry and Biochemistry, Tempe, AZ 85287, USA

Received 1 May 2007, in final form 21 June 2007
Published 27 September 2007
Online at stacks.iop.org/JPhysCM/19/415103

Abstract

The x-ray structure factor of vitreous As_2O_3 has been measured at 32 GPa in a laser-perforated diamond anvil cell using a monochromatic, micro-focused high-energy x-ray beam. The experimental correction procedures are discussed in detail, and they yield reliable data over the range $Q = 0.3$–13.5 Å^{-1}. The use of modified form factors to analyse the scattering data is presented to account for charge transfer. Analysis of the radial distribution function yields an increase in the coordination number from 3.1 ± 0.3 oxygen atoms surrounding an arsenic atom at normal pressure to 4.8 ± 0.5 at 32 GPa with only a slight change in the As–O bond length. Substantial structural changes are observed at higher distances, extending up to 18 Å in real space.

1. Introduction

The use of high-energy diffraction for the study of liquid and amorphous materials has grown in popularity in the past decade since the pioneering work of Poulsen and Neuefeind in the mid-1990s [1]. This is due in part to the advent of third-generation synchrotron sources such as the Advanced Photon Source (APS), and the ability to produce high-intensity monochromatic x-ray beams of $\geqslant$100 keV in energy. Moreover, high-energy total-scattering techniques at high pressures have become feasible in recent years, first using Ge solid-state detectors [2] and quickly followed by large-area detectors [3]. Some of the first experiments of this type were performed using $\sim$mm^3 size samples in the panoramic moissanite anvil cell [2, 4]. However, the technique suffered from a variation in the broad background with pressure, arising from changes in the diffuse scattering of the moissanite anvils, and in several cases these anvils failed catastrophically at pressures exceeding 10 GPa. Image plate area detectors have provided increased statistics using the panoramic pressure cell, providing a means of characterizing the change in background with pressure; however, the experiments remain challenging [5].

Advances in high-energy x-ray focusing optics now enable the use of high-pressure experiments on glasses and liquids using diamond anvil cells (DACs) [3] allowing a much larger range of pressure to be explored. However it is shown that Compton scattering from

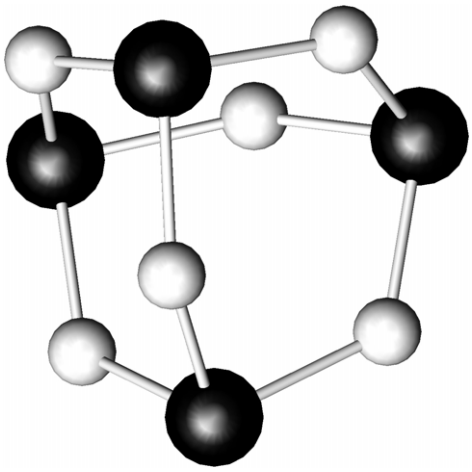

Figure 1. The As_4O_6 molecule.

DACs can overwhelm the signal at high Q, especially for samples containing light elements. In addition, the sample amount is small (and therefore the signal) compared to the volume of diamond. This has been circumvented to a significant extent by the use of mechanically perforated diamond anvils [6, 7]. However, in our experience high-energy x-ray experiments above 15 GPa using these mechanically perforated anvils have not been possible. In this paper we present the use of laser-perforated anvils, allowing us to achieve DAC pressures of >30 GPa, using the example of vitreous As_2O_3. The high-pressure structure of vitreous As_2O_3 (v-As_2O_3) is of interest because Raman studies have indicated that a structural transition occurs around a pressure of 27 GPa [8].

High-energy diffraction studies on compressed samples of v-As_2O_3 (recovered to normal pressure) have shown that AsO_3 pyramids, which dominate the ambient pressure glass structure, are relatively rigid under pressure [9]. The densified samples exhibit only a very slight elongation of the As–O bond and hardly any change in the As–As distance between AsO_3 pyramids. The main changes in the radial distribution functions of glasses recovered from 10 and 23 GPa appear as a decrease in the distance between second and third nearest-neighbour AsO_3 units with increasing density. This suggests that the principal compression mechanisms at lower pressures are likely to be associated with a denser packing of AsO_3 units. Our previous experiments using the panoramic cell failed to yield a structure factor for the reasons described above. However, it was observed that the first sharp diffraction peak reduces in intensity up to 10 GPa, indicating a breakdown of intermediate-range order with pressure [9]. *In situ* high-pressure Raman measurements up to 11.6 GPa show that the mode at 378 cm^{-1}, associated with As_4O_6 molecule-like vibrations (see figure 1), increases in intensity up to 6.2 GPa before diminishing in intensity at higher pressures.

This paper outlines the data analysis procedures used for obtaining the x-ray structure factor $S(Q)$ from high-pressure image plate data using vitreous As_2O_3 as an example. The effect of charge transfer and the use of modified atomic form factors are considered.

2. Experimental details

Vitreous As_2O_3 was made by sealing arsenolite (Aldrich, 99.999%) in a quartz tube and heating to 800 °C for 2 h. The thermostat of the furnace was lowered to 100 °C and the sample was allowed to cool for 1 h before quenching in an ice/water slurry to obtain vitreous As_2O_3.

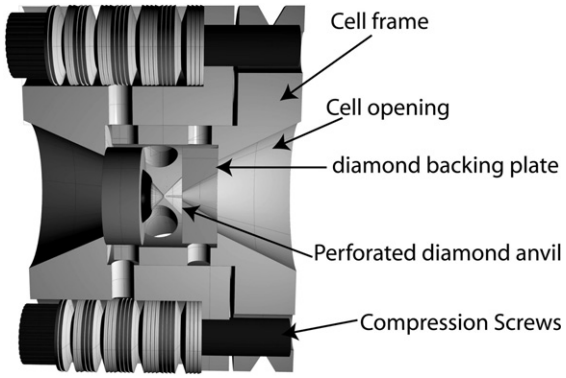

Figure 2. Three-dimensional illustration of a perforated diamond anvil cell.

The *in situ* high-pressure x-ray diffraction measurements were conducted on beamline 1-ID at the APS, using a cryogenically cooled bent double-Laue monochromator [10] with an incident beam of area 50 × 50 μm^2 and high incident beam energy of 100.0 keV. Pressure was applied to the sample using a cylindrical diamond anvil cell (DAC) with WC diamond anvil supports, allowing reliable diffraction patterns to be taken in a large solid angle up to a maximum scattering angle 2θ of 20°. The DAC was fitted with 300 μm culet anvils (type I) of length 1.8 mm and a rhenium gasket (250 μm in thickness) was pre-indented to 30 μm. A sample chamber, 100 μm in diameter, was drilled into the pre-indented gasket by using a micro-electro-discharge machining technique, creating a cavity of $\sim 3 \times 10^{-4}$ mm^3, which housed the glassy As_2O_3; see figure 2. Two ruby crystals, each of volume about 10 μm^3, were placed in the sample container to determine the pressure using the ruby fluorescence technique [11], to within an accuracy of ±10%.

An incident beam energy of 100 keV scattered from the sample into an a-Si GE Revolution area detector. The detector was exposed for 100 intervals of 10 s to avoid saturation due to the anvil Bragg peaks. These runs were averaged to improve the counting statistics.

3. Data analysis

3.1. Anvil scatter

Laser-perforated diamonds were used to minimize the amount of anvil material in the beam path and thereby the Compton scattering from the DAC, while maintaining a relatively high strength. Figure 3 compares the intensity of Ge–Se glasses versus that of the normal DAC and perforated DAC. As shown in the figure, the signal to noise ratio can be improved substantially by using perforated DACs for chalcogenide glasses. Utilizing perforated DACs in high-energy x-ray experiments is even more important in determining the high-pressure structure of oxide glasses and other light-element systems. However, DACs contribute many single-crystal diamond peaks to the diffraction pattern, as can be seen in the two-dimensional (2D) image from the image-plate detector in figure 4, which also shows the single-crystal ruby Bragg scattering from the pressure sensors. The vicinity surrounding the Bragg peaks was carefully deleted from the image plate detector by identifying regions of intensity above a certain threshold and enlarging these regions using the program *FIT2D* [12, 13]. In some cases, this process can be problematic if the cell is removed and replaced in a slightly different orientation between runs, which can rotate the crystal spots or affect the minimum Q-value. Ideally, the same

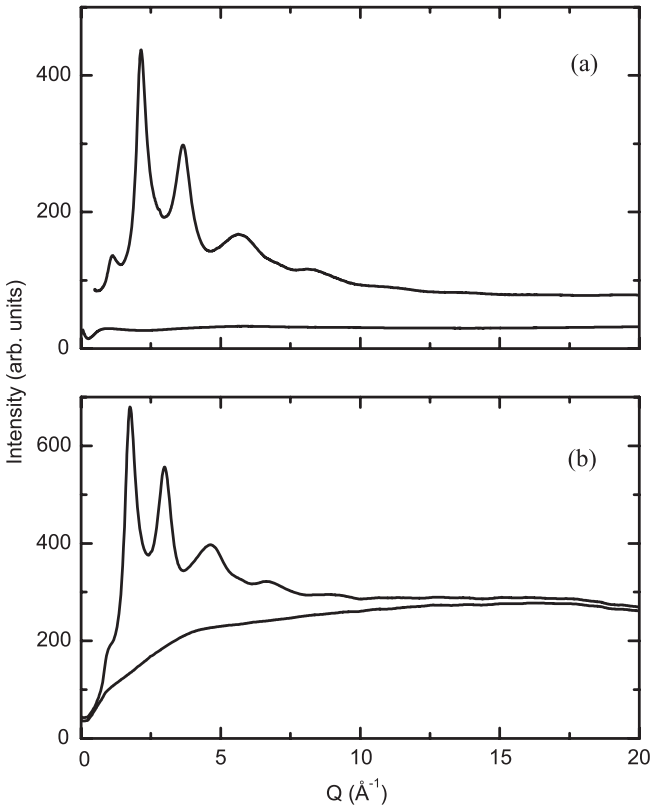

Figure 3. (a) The raw intensity measured using high-energy x-rays for glassy $GeSe_2$ in a perforated DAC at 5.3 GPa (upper curve) and for the empty DAC at ambient pressure (lower curve); (b) the raw intensity measured using high-energy x-rays for glassy $GeSe_4$ in a DAC at 6.0 GPa (upper curve) and for the empty DAC at ambient pressure (lower curve).

software mask needs to be applied to data on the sample and on the background to ensure the best background subtraction. A beam polarization correction is also made to the 2D data. A geometrical correction to the measured intensity is made by measuring a known crystalline standard (e.g. CeO_2) within the DAC to obtain the exact sample to detector distance for a beam of known energy, such that the data can be placed on the correct Q-scale [12, 13]. The minimum Q-value was affected slightly between the sample and background runs, probably due to the cell not being mounted precisely in the same position, so data below $Q < 0.5$ Å^{-1} were not used.

4. Data corrections

The data on an image plate may be reduced to intensity versus scattering angle with a small Q bin-width of $\Delta Q \sim 0.005$ Å^{-1}, compared to a more typical value of $\sim$0.025 Å^{-1} for solid-state Ge detector measurements. The background intensity collected for the empty DAC with no applied pressure was used as the background for the *in situ* high-pressure experiment at 32 GPa. Unlike our previous studies with a panoramic moissanite anvil pressure cell [2], there were no noticeable changes in the diffuse scattering of the diamonds with increasing pressure and, therefore, no additional correction for pressure-dependent anvil stress was needed.

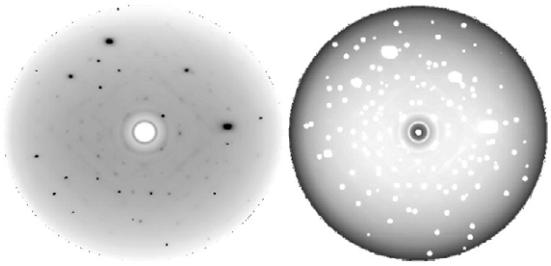

Figure 4. Left: raw 2D detector image for As_2O_3 glass in a DAC at 32 GPa. The black spots represent single-crystal peaks from the diamond anvils and the As_2O_3 glass appears most clearly in inner diffuse rings. Right: the same image inverted in greyscale with a software mask applied to eliminate the single-crystal peaks. The mask appears as white regions.

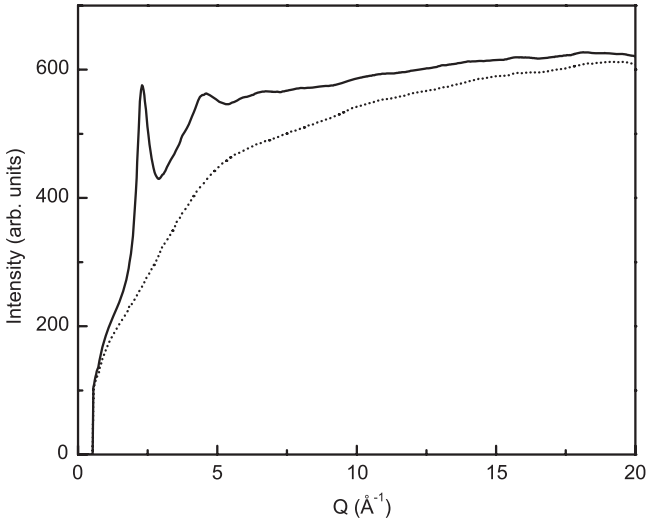

Figure 5. Raw integrated intensity of the As_2O_3 signal at normal pressure versus that of the empty cell multiplied by the attenuation factor 0.94.

The data analysis and corrections were based on the following equation, to yield the x-ray structure factor $S(Q)$:

$$S(Q) - 1 = \left(\beta \frac{I_S(Q) - A I_B(Q)}{K(Q)} - \sum_i c_i f_i^2(Q) - \sum_i c_i C_i(Q)\right) \Bigg/ \left[\sum_i c_i f_i(Q)\right]^2 \quad (1)$$

where $I_S(Q)$ represents the scattered intensity of the sample plus background at high pressure and $I_B(Q)$ is the scattered intensity of the empty DAC with no pressure applied.

A represents the attenuation factor, which typically has the form $A = 1 - \exp(-\mu t/\cos 2\theta)$ for a flat-plate DAC geometry orientated perpendicular to the beam, where t is the thickness and μ the attenuation coefficient of the diamond and 2θ is the scattering angle [14, 15]. However, this factor was found to be essentially constant in this analysis over the small angular range (see figure 5).

β is the scaling factor required to normalize the data to the Laue diffuse scattering $\sum_i c_i f_i^2(Q)$ plus Compton scattering $\sum_i c_i C_i(Q)$ at high Q. Here c_i is the concentration of atomic species i.

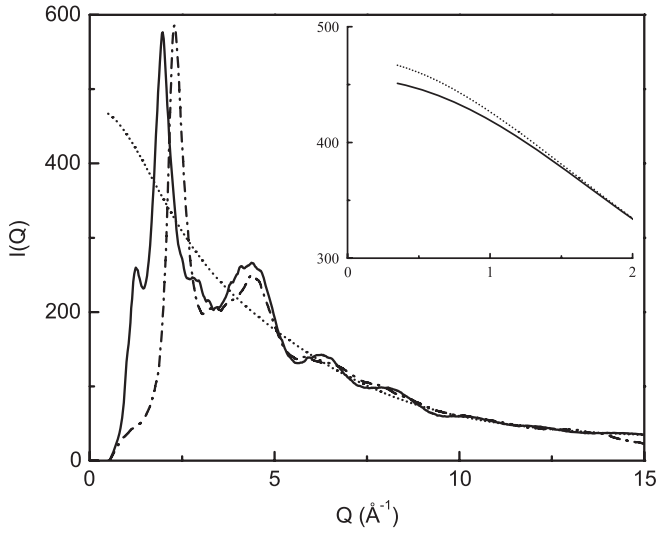

Figure 6. High-energy x-ray intensity for As_2O_3 at normal pressure (solid line) and 32 GPa (dash–dotted line), which is normalized to Compton scattering and form factors (dotted line). The inset figure compares the Laue scattering $\sum_i c_i f_i^2(Q)$ based on free-atom form factors (short dotted line) and modified atomic form factors (solid line in the insertion) in the low-Q region.

Standard tabulated values for the Q-dependent Compton scattering, $C(Q)$, and atomic x-ray form factors, $f_i(Q)$, were taken from the Hubbell *et al* fit to 4-Gaussian peaks [16]. However, in this analysis the atomic $f_i(Q)$ were replaced with modified form factors $f_i'(Q)$, as described later. $K(Q)$ is the oblique incidence correction arising from the angle-dependent path length absorption through the image plate phosphor [17]. $K(Q)$ can be calculated according to the following equation:

$$K(Q) = \frac{\left\{1 - \exp\left[(\ln T_\perp)/\cos\left(2 \cdot \sin^{-1}(Q \cdot \lambda/4\pi)\right)\right]\right\}}{1 - T_\perp} \tag{2}$$

where $T_\perp$ is the transmission of the phosphor layer at the normal incidence, and is taken as 0.98 in this case.

5. Results and discussion

Figure 5 shows the corrected integrated intensity of the As_2O_3 glasses at 32 GPa versus that of the empty cell multiplied by a constant attenuation factor $A = 0.94$. The intensity of the empty cell signal is at least ten times higher than that of the sample signal at $Q = 20$ Å^{-1}, but this improves towards lower Q-values. This dominant signal is associated with the Compton scattering from the diamond anvils. Figure 6 shows the term $\beta \frac{I_S(Q) - AI_B(Q)}{K(Q)}$ normalized to the atomic form factor plus Compton scattering at high Q, $\sum_i c_i f_i^2(Q) + \sum_i c_i C_i(Q)$ for As_2O_3 glass at ambient pressure and 32 GPa. The diffraction data deviate from this calculated line above $Q = 13.5$ Å^{-1}. The deviation cannot be accounted for by the change in attenuation coefficient for flat-plate geometry, but most likely arises from an incorrect subtraction of the diamond anvil Compton scattering at high Q, yielding a reliable $S(Q)$ at high pressure over the restricted Q-range 0.3–13.5 Å^{-1}. This Q-range has been extended up to 17 Å^{-1} for experiments on materials containing heavier elements, i.e. $GeSe_2$ glass, using a similar

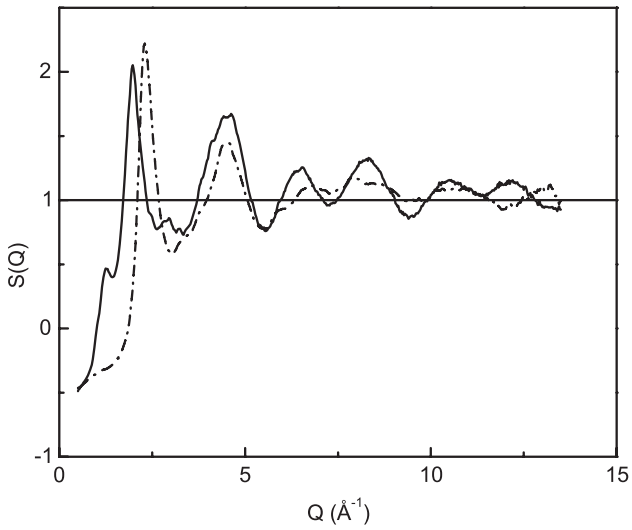

Figure 7. The total structure factors for As_2O_3 glass at 32 GPa (dash–dotted line) and ambient pressure (solid line) analysed using free-atom form factors.

experimental arrangement [3]. We note that no pressure medium was used in these experiments. The addition of a pressure medium would complicate the background subtraction and has not yet been attempted. However, the lack of a pressure medium results in non-hydrostatic pressure which is sample dependent (the shear modulus of the material will dictate the pressure gradient in the DAC). Using the pressure calculated from the fluorescence of several ruby chips placed in the sample chamber, we estimated a pressure gradient of ∼3 GPa within the volume of sample probed by the x-ray beam. The average pressure in the DAC was 32 GPa. The corrected high-pressure x-ray structure factor for As_2O_3 glass is compared to that obtained at ambient pressure in figure 7, measured outside the cell using an energy-discriminating solid-state Ge detector, on beamline 11 IDC at the APS, up to a Q-value of 25 Å^{-1} [9].

6. Compressibility limit, charge transfer and $S(Q)$ at low Q

For a homogeneous system, assuming that density fluctuations frozen in at the glass transition temperature T_g are governed only by the diffusive part of the isothermal compressibility, the corrected x-ray intensity may be written as [18]

$$I(Q=0) = \rho K_B T \chi_T \left(T_g\right) \sum_i c_i f_i'^2(0), \tag{3}$$

where ρ represents the number density, $\chi_T(T_g)$ is the isothermal compressibility of the supercooled liquid at T_g and the $f_i'(Q)$ represent the modified atomic form factors.

It has been suggested by Head-Gordon and co-workers [19] that the low-Q behaviour of the free-atom form factors may be improved to a first approximation by a simple scaling of the individual atomic form factors, and that is the approach adopted here. The atomic form factors are modified at low Q to account for bonding effects, while keeping the accurate free-atom approximation at high Q [19]. Given that q is the transfer of charge onto each oxygen atom, we write the modified atomic form factor (MAFF), $f_o'(Q)$, for oxygen as

$$f_O'(Q) = \left[1 - \frac{q}{Z_O} \exp\left(-Q^2/2\delta^2\right)\right] f_O(Q). \tag{4}$$

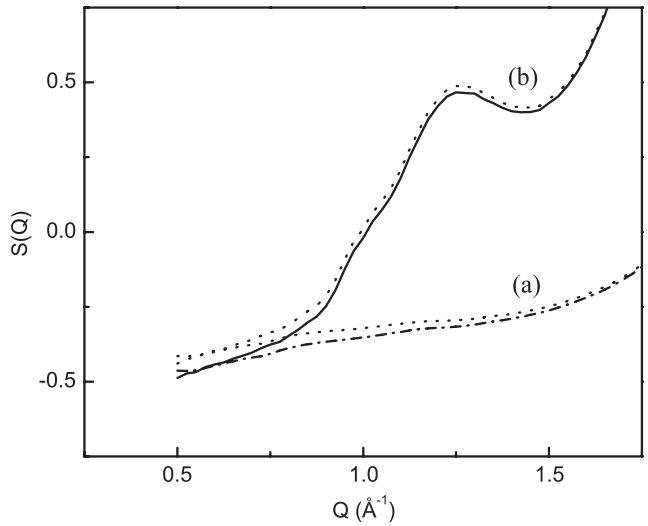

Figure 8. (a) The total structure factors for As_2O_3 glass at 32 GPa with normal form factors (dash–dotted line) and with modified form factors (dotted line); (b) the total structure factor at ambient pressure with normal form factors (solid line) and with modified form factors (dotted line).

Similarly, the modified atomic form factor for the As atom is given by

$$f'_{\mathrm{As}}(Q) = \left[1 + \frac{c_{\mathrm{O}} q}{c_{\mathrm{As}} Z_{\mathrm{As}}} \exp\left(-Q^2/2\delta^2\right)\right] f_{\mathrm{As}}(Q), \tag{5}$$

where $Z_{\mathrm{O}} = 8$ and $Z_{\mathrm{As}} = 33$, the parameter δ is a width function and $f_{\mathrm{O}}(Q)$ is the free-atom form factor. Overall charge neutrality of the system is preserved in equations (4) and (5). The amount of charge transfer $q = -0.6$ from arsenic to oxygen was estimated from first-order perturbation theory for the adamantine molecule As_4O_6 [20] (see figure 1). The parameter δ, which controls the crossover between the low-Q and high-Q limits was estimated from a comparison of the charged-ion form factors for Ge^{4+} and O^{2-} compared to their corresponding free-atom counterparts [21]. Both yielded a value of $\delta = 0.8$. The resulting structure factors $S'(Q)$ are slightly raised in the low-Q part of the spectra, as shown in figure 8.

Figure 9 compares the normalized Faber–Ziman partial weighting factors for As–O, As–As and O–O calculated using the free-atom and modified atomic form factors, where the measured x-ray structure factor,

$$S(Q) = \frac{c_{\mathrm{As}}^2 f_{\mathrm{As}}^2(Q) S_{\mathrm{AsAs}}(Q) + 2c_{\mathrm{As}} c_{\mathrm{O}} f_{\mathrm{As}}(Q) f_{\mathrm{O}}(Q) S_{\mathrm{AsO}}(Q) + c_{\mathrm{O}}^2 f_{\mathrm{O}}^2(Q) S_{\mathrm{OO}}(Q)}{c_{\mathrm{As}}^2 f_{\mathrm{As}}^2(Q) + 2c_{\mathrm{As}} c_{\mathrm{O}} f_{\mathrm{As}}(Q) f_{\mathrm{O}}(Q) + c_{\mathrm{O}}^2 f_{\mathrm{O}}^2(Q)}, \tag{6}$$

and the $S_{ij}(Q)$ are the partial structure factors. As can be seen in the figure, the major difference lies in the low-Q part, i.e. below 2 Å^{-1}, lowering the low-Q limit of the O–O and As–O Faber–Ziman weighting factors and raising the As–As weighting factor.

7. High-pressure As_2O_3

The first sharp diffraction peak at 1.27 ± 0.01 Å^{-1}, which is generally associated with intermediate-range order in the glass, has disappeared by 32 GPa. The principal peak at 1.98 ± 0.01 Å^{-1} is at 2.30 ± 0.01 Å^{-1}, and it has slightly increased in intensity. The significant

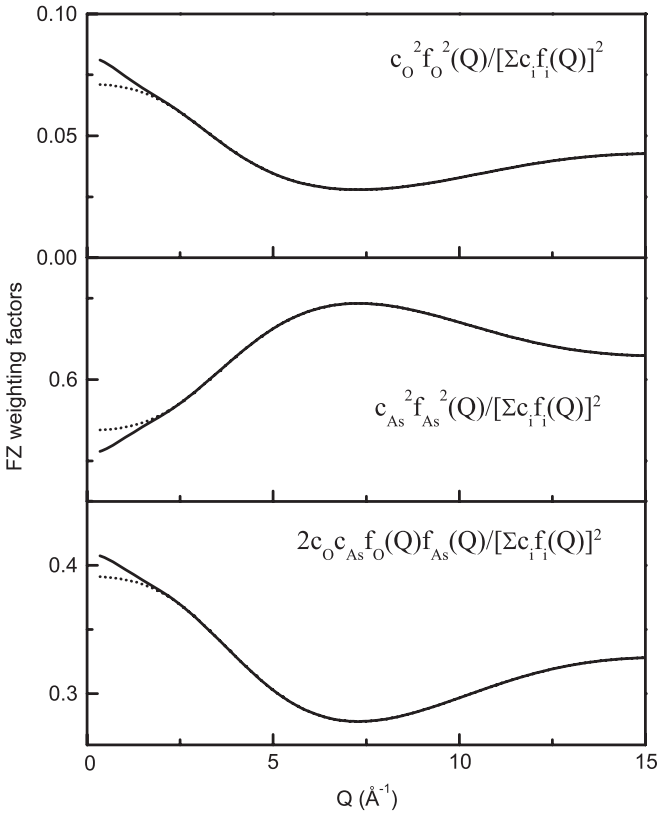

Figure 9. The normalized Faber–Ziman partial weighting factors for As–O, As–As and O–O calculated using the free-atom (dotted line) and modified atomic form factors (solid line), where i = As, O.

changes in the higher-Q oscillations above 5 Å^{-1} indicate that the short-range order structure goes through a major change under pressure.

Figure 10 shows the total pair distribution functions $D(r)$ for As_2O_3 glass at 32 GPa and ambient pressure, where $D(r) = 4\pi\rho r[G(r) - 1]$, highlighting the higher-r structure. The first peak at 1.77(1) Å arises from As–O bonds and the second peak at 3.18(1) Å arises from As–As correlations at ambient pressure. It is found that the As–O bond elongates slightly to 1.81(1) Å at 32 GPa and the As–As correlation distance shortens to 3.12(1) Å with significant broadening, and a high-r shoulder appears. The most drastic short-range order changes occur in the position of the peak located at 4.2 Å in the normal-pressure glass. This peak is assigned to third-neighbouring As–As/As–O correlations in the ambient pressure glass, and only a shoulder is observed at ∼4 Å at 32 GPa. The higher-r peaks are at 6.9, 10.3, 13.5, ∼16 and 19.5 Å in the ambient-pressure glass, whereas a new high-density network forms at 32 GPa with peak positions at 5.8, 8.7, 11.6, 14.3 and 17.3 Å.

8. Coordination number

It has been pointed out by Soper [22] that the Q-dependent form factors in equation (1) may yield some spurious structure in real space, and consequently experimentalists must be careful

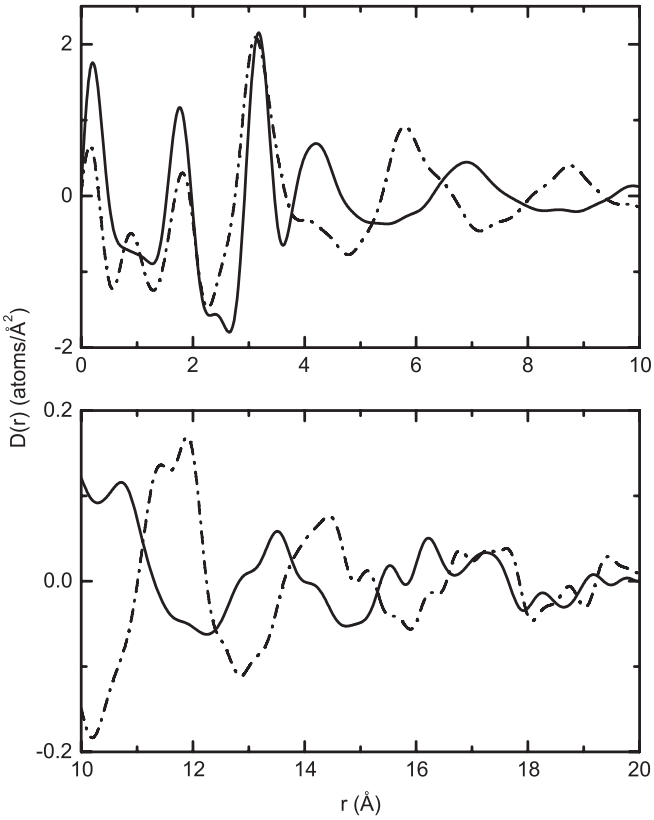

Figure 10. The total pair distribution functions $D(r) = 4\pi\rho r[G(r) - 1]$, for As_2O_3 glass at 32 GPa (dash–dotted line) and ambient pressure (solid line). The curves were obtained by Fourier transforming the total structure factors of figure 7 after the data sets were truncated at $Q_{max} = 13.5$ Å^{-1}. A Lorch function was applied to reduce Fourier artefacts.

when interpreting the x-ray $G(r)$ directly. In this analysis a Gaussian peak corresponding to a known number of oxygens around arsenic was Fourier transformed from r-space to Q-space, and convoluted with the normalized As–O Faber–Ziman x-ray weighting factor based on our MAFF analysis. The resulting Q-space function was Fourier transformed back into real space using a same maximum Q-value as the data and compared to the measured $G(r)$. This procedure was iterated until good agreement for As–O peak was obtained. The result of this analysis revealed that the number of oxygen atoms surrounding As rises from 3.1 ± 0.3 (using a density of $\rho = 0.0566$ atoms Å^{-3} [9]) at normal pressure to 4.8 ± 0.5 at 32 GPa (using $\rho = 0.103$ atoms Å^{-3} [23]).

Only slightly different results were obtained for the radial distribution function, $G(r)$, using the free-atom form factors and the modified atomic form factors described in the previous section. Specifically, the value of $\delta = 0.8$ slightly affected the low-r region around the first real peak in r-space when compared to the same curve obtained using the free-atom approximation. The MAFF analysis has no discernable effects in area of the first peak in the function r^2. $G(r)$ for the As_2O_3 glass at normal pressure and 32 GPa compared to that obtained using the free-atom approximation. Therefore, the coordination number remains the same, independent of the x-ray form factor we used.

Raman and infrared studies by Lucovsky *et al* [24] suggest that the As_2O_3 glass network has both arsenolite (As_4O_6 molecular-like) regions and claudetite (layer-like) regions, although neutron diffraction measurements by Clare *et al* [25] have indicated that arsenolite-like regions dominate the structure based on the torsion angles. The phonon spectra of crystalline arsenolite up to pressures of 16 GPa have been interpreted as a result of an enhancement of intermolecular interactions between As_4O_6 molecules [26]. On this basis, Grzechnik has proposed that the structural changes at low pressures take place in claudetite-like regions rather than in arsenolite-like regions. This is consistent with our published Raman data on As_2O_3 glass up to 6.2 GPa, which shows the increased intensity in the vibrational modes that are associated with As_4O_6 molecules [9]. From this analysis we find that the As–O bond length is relatively insensitive to the coordination number at higher pressures. Consequently, the x-ray data cannot be used to determine if the structure consists of a mixture of 3-, 4-, 5- and 6-coordinated polyhedra or is simply a mixture of 3- and 6-coordinated polyhedra at higher pressure. Raman and infrared studies of As_2O_3 glass are needed to help elucidate the densification mechanisms at higher density.

9. Conclusions and future outlook

In summary, we present the successful use of a laser-perforated diamond anvil cell in combination of a micro-focused 100 keV x-ray beam, to obtain the structure factor of glassy As_2O_3 at 32 GPa up to 13.5 $Å^{-1}$. The technique offers a significant improvement over our previous (unsuccessful) attempts on this glass using a larger-volume panoramic cell [9]. A coordination number analysis shows an increase in the number of oxygens around arsenic atoms from 3.1 ± 0.3 at normal pressure to 4.8 ± 0.5 at 32 GPa. This is interpreted as a break up of AsO_3 units which dominate the normal glass structure and the formation of higher-coordinate As polyhedra in the high-density glass. Remarkably, this coordination change occurs with only a small elongation in the As–O bond length from 1.76 to 1.81 Å at high pressure. Substantial structural changes occur at larger r, extending out to distances up to at least 18 Å.

On the theme of current challenges in glass structure we show that considerable progress has been made in recent years in extracting high-quality x-ray structure factors at high pressures, even from weakly scattering oxide systems. Given the strong influence that density has on atomic structure it may be expected that this field will produce some interesting physics in the future, especially with regard to identifying densification mechanisms and structural transitions. This paper highlights three aspects of glass structure determination which need to be addressed. The first is extending the momentum transfer range for x-ray diffraction measurements. At $Q = 13.5$ $Å^{-1}$, we are near the minimum realistic limit for obtaining a reliable radial distribution function, and this needs to be extended.

A second issue of complementary techniques in glass structure determination also deserves to be mentioned. Accurate equation of state measurements are required to measure densities at high pressure to aid in the interpretation of the measured diffraction data. *In situ* Raman spectroscopy measurements up to 11.6 GPa have also provided a valuable source of local structural information in the As_2O_3 glass studied here [9]. A future publication is planned to interpret the detailed structural changes observed in high-pressure diffraction measurements from glassy As_2O_3 over a range of pressures, using equation of state data and new *in situ* high-pressure Raman measurements up to ∼32 GPa. Finally, with the advent of dedicated high-pressure neutron diffractometers at high-power spallation sources, measurements over a wide Q-range will provide additional important complementary structural information for glasses containing light elements such as As_2O_3.

Acknowledgments

This work is supported by the US Department of Energy, at the X-ray Science Division and the Intense Pulsed Neutron Source, Argonne National Laboratory under contract number DE-AC02-06CH11357. JLY would like to acknowledge the National Science Foundation, the Department of Energy and the Department of Defense, Army Research Office, for research funding.

References

[1] Poulsen H F *et al* 1995 *J. Non-Cryst. Solids* **188** 63
[2] Guthrie M, Tulk C A, Benmore C J, Xu J, Yarger J L, Klug D D, Tse J S, Mao H K and Hemley R J 2004 *Phys. Rev. Lett.* **93** 115502
[3] Mei Q *et al* 2006 *Phys. Rev.* B **74** 014203
[4] Xu J, Mao H, Hemley R J and Hines E 2002 *J. Phys.: Condens. Matter* **14** 11543
[5] Soyer S *et al J. Phys. Chem. Solids* submitted
[6] Parise J B, Antao S M, Michel F M, Martin C D, Chupas P J, Shastri S D and Lee P L 2005 *J. Synchrotron Radiat.* **12** 554
[7] Dadashev A, Pasternak M P and Rozenberg G Kh 2001 *Rev. Sci. Instrum.* **72** 2633
[8] Amin S and Yarger J L 2006 private communication
[9] Mei Q, Hart R T, Benmore C J, Amin S, Leinenweber K and Yarger J L 2007 *J. Non-Cryst. Solids* **353** 1755
[10] Martin C D, Antao S M, Chupas P J, Lee P L, Shastri S D and Parise J B 2005 *Appl. Phys. Lett.* **86** 061910
[11] Barnett J D, Block S and Piermarini G J 1973 *Rev. Sci. Instrum.* **44** 1
[12] Hammersley A P, Svensson S O, Hanfland M, Fitch A N and Häusermann D 1996 *High Pressure Res.* **14** 235
[13] Hammersley A P 1998 *Internal Report No. ESRF98HA01T, European Synchrotron Radiation Facility (Grenoble, France)* unpublished
[14] Soper A K 1983 *Nucl. Instrum. Methods* **212** 337
[15] Kasper J S and Lonsdale K (ed) 1989 *International Tables for Crystallography* vol II (Dordrecht: Kluwer) p 291 (section 5.3: Absorption corrections)
[16] Hubbell J H, Veigele Wm J, Briggs E A, Brown R T, Cromer D T and Howerton R J 1975 *J. Phys. Chem. Ref. Data* **4** 471
[17] Zaleski J, Wu G and Coppens P 1998 *J. Appl. Crystallogr.* **31** 302
[18] Wright A C and Zeil W 1974 *Advances in Structure Research by Diffraction Methods* vol 5, ed W Hoppe and R Mason (Braunschweig: Friedr. Wieweg/Sohn GmbH) p 42
[19] Sorenson J M, Hura G, Glaeser R M and Head-Gordon T 2000 *J. Chem. Phys.* **113** 9149
[20] Gimarc B M and Ott J J 1986 *J. Am. Chem. Soc.* **108** 4298
[21] *International Tables for Crystallography* 2006 vol C pp 554–90 section 6.1.1 (Note the charged form factor for As^{4+} is not given here)
[22] Soper A K 2007 *J. Phys.: Condens. Matter* **19** 335206
[23] The equation of state for As_2O_3 was been measured up to ∼32 GPa by using the method outlined in [3], unpublished
[24] Lucovsky G and Galeener F L 1980 *J. Non-Cryst. Solids* **37** 53
[25] Clare A G, Wright A C, Sinclair R N, Galeener F L and Geissberger A E 1989 *J. Non-Cryst. Solids* **111** 123
[26] Grzechnik A 1999 *J. Solid State Chem.* **144** 416–22